CH_3O Yield in the $CH_3 + O_3$ Reaction Using the LP/LIF Technique at Room Temperature

José Albaladejo,* Elena Jiménez, Alberto Notario, Beatriz Cabañas, and Ernesto Martínez

Departamento de Química Física, Facultad de Ciencias Químicas, Universidad de Castilla-La Mancha, Campus Universitario s/n, 13071 Ciudad Real, Spain

Received: June 14, 2001; In Final Form: October 17, 2001

$CH_3O(X^2E)$ radicals have been detected by laser-induced fluorescence (LIF) for the first time as a product of the reaction between CH_3 and O_3. CH_3 radicals were generated by excimer-laser photolysis of CH_3Br at 193 nm in the presence of O_3 at room temperature and 100 Torr of He. The rate constant for reaction 1a ($CH_3 + O_3 \rightarrow CH_3O + O_2$) has been determined by monitoring the CH_3O build-up as a function of reaction time and k_{1a} was found to be $(9.68 \pm 1.10) \times 10^{-14}$ cm^3 molecule^{-1} s^{-1}. The rate coefficient of the global reaction 1 ($CH_3 + O_3 \rightarrow$ products) has been determined by the numerical analysis of the CH_3O temporal profiles, yielding a value of $k_1 = (2.2 \pm 0.3) \times 10^{-12}$ cm^3 molecule^{-1} s^{-1}. Reaction of CH_3 with NO_2 has also been studied under the same experimental conditions as reaction 1 and has been used to calibrate the CH_3O LIF signal. On the other hand, the rate constant k_2 for reaction 2 ($CH_3O + O_3 \rightarrow$ products) has been directly determined ($k_2(T = 298\ \text{K}) = (2.53 \pm 0.75) \times 10^{-14}$ cm^3 molecule^{-1} s^{-1}) using the $CH_3ONO(\lambda = 193\ \text{nm})/O_3$/He system and was included in the chemical model used to describe the kinetics of CH_3 in the presence of O_3. The branching ratio $\phi_{CH_3O} = k_{1a}/k_1$ obtained was found to be (0.044 ± 0.013). This low yield of CH_3O in reaction 1a can be explained not only by the formation of highly vibrationally excited CH_3O and the subsequent prompt dissociation to produce $CH_2O + H$ but also by the direct formation of $CH_2O + HO_2$ in reaction 1.

1. Introduction

Despite the relevance of methyl radical, CH_3, in atmospheric chemistry, since this radical is produced in the earth's atmosphere by CH_4 oxidation, the nature of the products of the reaction of CH_3 with ozone, O_3,

$$CH_3 + O_3 \xrightarrow{k_1} \text{products} \qquad (1)$$

is still a matter of speculation. The kinetics of reaction 1 has been the subject of several direct[1,2] and indirect studies.[3] Simonaitis and Heicklen[3] performed a kinetic study of reaction 1 by measuring the quantum yield of O_3 removal as a function of the O_3/O_2 ratio at +25 and −52 °C and at a pressure of about 1 atm. These authors photolyzed O_3 at $\lambda = 253.7$ nm in the presence of CH_4 and O_2. The chemical complexity of that system and the treatment of the proposed mechanism gave only an estimation of the rate constant of the above reaction. On the other hand, an upper limit for the rate constant of the reaction of CH_3O radical with O_3 in the same chemical system ($O_3(\lambda = 253.7\ \text{nm})/CH_4/O_2$)

$$CH_3O + O_3 \xrightarrow{k_2} \text{products} \qquad (2)$$

was determined indirectly by Simonaitis and Heicklen.[3] More recently, Washida et al.[1] carried out a room temperature study of the $CH_3 + O_3$ reaction at low pressures ($p_T = 2-6$ Torr of He), using a discharge-flow system coupled to a mass spectrometry detection system. The reaction of O atoms with C_2H_4 used to generate methyl radicals is thought to be more complicated than was initially assumed. Finally, the last kinetic study of the $CH_3 + O_3$ reaction was also performed using low total pressures ($p_T = 2.2 \pm 0.2$ Torr in He) by Ogryzlo et al.[2] as a function of temperature ($T = 243-384$ K). Laser photolysis of nitromethane, CH_3NO_2, at 193 nm was employed as a source of CH_3 radicals, and photoionization mass spectrometry was used to follow the CH_3 decay rate at various ozone concentrations.[2] Information regarding the products was not given in the above study, and the room temperature rate constant reported is approximately three times greater that those obtained in the two previous studies.

In the work described here, kinetic studies of CH_3 and CH_3O radicals with O_3 were carried out at room temperature and with a total pressure of 100 Torr in He. The experiments involved laser-pulsed photolysis (LP) of a suitable precursor to generate the transient species and laser-induced fluorescence (LIF) to monitor $CH_3O(X^2E)$ as a function of reaction time. A numerical simulation of the CH_3O concentration profiles was performed in order to derive k_1. Furthermore, we report the first direct determination of the rate constant of the reaction $CH_3O + O_3$ (k_2) as well as the CH_3O yield in reaction 1 for the reaction channel,

$$CH_3 + O_3 \xrightarrow{k_{1a}} CH_3O + O_2 \qquad (1a)$$

obtained by fitting the rate data to the simulated profiles and varying only the absolute rate constant for this route, k_{1a}, under the same experimental conditions.

Determinations of the rate constant k_{1a} and the branching ratio of $CH_3O(X^2E)$ formation in reaction 1, k_{1a}/k_1, are achieved by comparing the time dependence of the CH_3O LIF signal with that recorded, under the same experimental conditions, in the reaction of CH_3 with NO_2, to calibrate the CH_3O LIF signal.

* Phone: +34 9 26 29 53 00. Fax: +34 9 26 29 53 18. E-mail: Jose.Albaladejo@uclm.es.

10.1021/jp012249o CCC: $22.00
Published on Web 02/13/2002

The reaction of CH_3 with NO_2 is known to proceed via two channels, a pressure independent channel,

$$CH_3 + NO_2 \rightarrow CH_3O + NO \quad (3a)$$

and a pressure-dependent channel:

$$CH_3 + NO_2 + He \rightarrow \text{products} + He \quad (3b)$$

CH_3O radicals formed in reaction 3a react rapidly with NO_2 present in the reaction cell via the following processes:

$$CH_3O + NO_2 \rightarrow CH_2O + HONO \quad (4a)$$

$$CH_3O + NO_2 + He \rightarrow \text{products} + He \quad (4b)$$

For this reason, kinetic data for both reactions 3 and 4 are required to analyze CH_3O temporal profiles obtained for the reference reaction. Analysis of the CH_3O temporal profiles yields the rate constant for the recombination reaction 3b as a function of total pressure ($p_T = 20-311$ Torr in He) at room temperature.

2. Experimental Section

All experiments were carried out using pulsed laser photolysis in combination with a pulsed laser-induced fluorescence technique (LP−LIF). Details of the experimental setup were previously described in recent publications regarding CH_3S[4,5] and CH_3O[6] radicals. A brief description of the experimental system and conditions is given below.

Photolysis of an appropriate precursor (commercial CH_3Br or synthesized CH_3ONO) using the pulsed 193-nm radiation of an ArF-excimer laser (OPTex, Lambda Physik), with fluences in the range 0.4−3 mJ pulse^{-1} cm^{-2}, was used as a source of CH_3 and CH_3O radicals, respectively:

$$CH_3Br + h\nu(\lambda = 193\ \text{nm}) \rightarrow CH_3 + Br \quad (5)$$

$$CH_3ONO + h\nu(\lambda = 193\ \text{nm}) \rightarrow CH_3O + NO \quad (6)$$

Because the CH_3 radical cannot be detected by LIF, the conversion of this radical into CH_3O in the presence of NO_2 or O_3 was used to monitor its kinetics in the reactions described here. A Nd:YAG-pumped frequency-doubled dye laser (Continuum ND60 and NY81CS-10) was used to monitor the CH_3O concentration decay or build up, generated either directly or indirectly, by exciting CH_3O radicals at $\lambda = 292.4$ nm:[7]

$$CH_3O(X^2E) + h\nu\ (\lambda = 292.4\ \text{nm}) \rightarrow CH_3O(A^2A_1) \quad (7)$$

The resulting red-shifted fluorescence was subsequently collected at a right angle with respect to the excitation and photolysis beams in a photomultiplier tube (Thorn EMI, 9813B) coupled to the Pyrex reaction cell. A band-pass filter (Schott, BG5) or an interference filter centered at $\lambda = 360$ nm (Andover) was used to monitor the CH_3O LIF signal.

The kinetic studies of CH_3 and CH_3O radicals were carried out at room temperature under a total pressure of 100 Torr, and always under pseudo-first-order conditions with respect to the initial concentration of the radical generated in the photolysis. In the study of CH_3O formation by reaction 1a, the photolysis of CH_3Br ($[CH_3Br] = (1.9-9.8) \times 10^{14}$ molecule cm^{-3}) generated CH_3 radicals ($[CH_3]_0 = (0.7-3.1) \times 10^{12}$ radical cm^{-3}) in the presence of an excess of O_3 ($[O_3] = (0.5-5.8) \times 10^{14}$ molecule cm^{-3}). The absorption cross section of CH_3Br at 193 nm used[8] was 5.75×10^{-19} cm^2, and the quantum yield for CH_3 formation was taken to be unity.[9] The CH_3O buildup due to reaction 1a was also monitored by LIF. The same experimental conditions and concentrations were used in the study of the calibration process $CH_3 + NO_2$.

The diffusion of CH_3 and CH_3O radicals out of the detection zone constitutes only a minor channel at the experimental pressure used. However, this possibility was also considered:

$$CH_3 \rightarrow \text{diffusion} \quad (8)$$

$$CH_3O \rightarrow \text{diffusion} \quad (9)$$

In the kinetic study of the reaction $CH_3O + O_3$, the typical concentrations of the photochemical precursor used were $[CH_3ONO] = (0.35-2.14) \times 10^{15}$ molecule cm^{-3}, giving $[CH_3O]_0 = (1.3-9.8) \times 10^{11}$ radical cm^{-3} ($\sigma_{CH3ONO}(\lambda = 193\ \text{nm}) \sim 2 \times 10^{-18}$ cm^2).[10] The ozone concentrations employed in these experiments were in the range $(0.11-4.47) \times 10^{15}$ molecule cm^{-3}.

Photolysis of O_3 present in the system at 193 nm ($\sigma_{O3}(\lambda = 193\ \text{nm}) = 4.28 \times 10^{-19}$ cm^2)[11] generates ground- and excited-state O atoms, O^3P and O^1D, with quantum yields of 0.57 ± 0.14 and 0.46 ± 0.29, respectively.[12] Typical total initial concentrations of atomic oxygen ($[O^3P] + [O^1D]$) were in the range $(0.053-4.00) \times 10^{12}$ atoms cm^{-3}. The influence of these concentrations of atomic oxygen in the kinetic measurements is considered in the analysis of the results.

Reagents. Helium carrier gas (Carburos Metálicos, 99.999%) was used without further purification. NO_2 and CH_3Br were taken from cylinders (Praxair, >99.5%) and were degassed by repeated distillation at low temperatures. The ArF gas mixture for the excimer laser was prepared by Praxair with the required specifications of Lambda Physik. Ozone was synthesized in a commercial ozonizer (Ozogas, TRCE−5000) and trapped in a liquid nitrogen trap, which was continuously pumped to remove any O_2 present and then was highly diluted in He (<1%). The exact O_3 concentration in the mixture was determined by its optical absorption at 253.7 nm in a 110 cm absorption cell located upstream of the photolysis reactor. This measurement was also used to derive the O_2 concentration present in the aged O_3 mixtures. Comparing the calculated $[O_3]$ in the mixture with the value determined by optical absorption, we estimated $[O_2] \cong 8 \times 10^{14}$ cm^3 molecule^{-1} s^{-1} inside the reactor at the highest $[O_3] \cong 4 \times 10^{15}$ cm^3 molecule^{-1} s^{-1}. Usually $[O_2]$ was much less because $[O_3]$ was smaller and O_3 mixtures were freshly prepared frequently. Samples of CH_3ONO were freshly prepared by the dropwise addition of a 50% H_2SO_4/water solution to a 50% methanol/water solution that was saturated with $NaNO_2$. The reaction vessel was cooled in an ice bath, and the resultant gaseous product was dried by passage through Na_2CO_3 and molecular sieves. The gas was then collected at −50 °C. The CH_3ONO contained in the trap was transferred to a vacuum line and thoroughly purified by freeze−pump−thaw cycles and then highly diluted (0.6−1%).

3. Results

The results obtained in this work are described in three separate sections: $CH_3 + NO_2$ calibration reaction, $CH_3O + O_3$ reaction, and $CH_3 + O_3$ reaction.

3.1. Kinetics of the $CH_3 + NO_2$ Reaction: CH_3O Calibration. Figure 1 shows two examples of the CH_3O temporal profiles generated by photolysis of CH_3Br at 193 nm in the presence of different concentrations of NO_2 at $T = 298$ K and

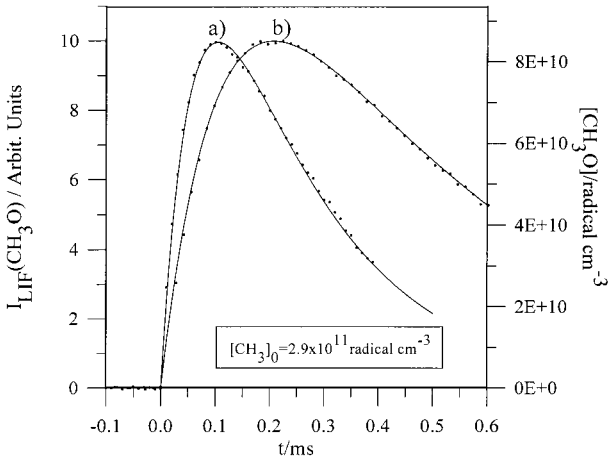

Figure 1. CH_3O temporal profiles obtained in the 193 nm photolysis of $[CH_3Br] = 1.2 \times 10^{14}$ molecule cm^{-3} at 298 K and 100 Torr, in the presence of (a) $[NO_2] = 3.3 \times 10^{14}$ and (b) 1.6×10^{14} molecule cm^{-3}.

TABLE 1: Reaction Mechanism Used in the Numerical Simulation of the CH_3Br(λ = 193 nm)/NO_2/He System at T = 298 K and p_T = 100 Torr

reaction	k (cm^3 molecule^{-1} s^{-1})	reference
$CH_3 + NO_2 \rightarrow CH_3O + NO$	$k_{3a} = 2.5 \cdot 10^{-11}$	14
$CH_3 + NO_2 + He \rightarrow$ products + He	k_{3b} = variable	this work
$CH_3O + NO_2 \rightarrow CH_2O + HONO$	$k_{4a} = 2 \cdot 10^{-13}$	13
$CH_3O + NO_2 + He \rightarrow CH_3ONO_2 + He$	$k_{4b} = 1.41 \cdot 10^{-11}$	6
$CH_3 \rightarrow$ diffusion	$k_{diff} = 50^a$	this work
$CH_3O \rightarrow$ diffusion	$k_{diff} = 50^a$	6

[a] First-order rate coefficients, in inverse seconds.

100 Torr. Solid lines represent CH_3O concentration profiles numerically simulated using the FACSIMILE computer program. Variation of the NO_2 concentration is seen to influence the time at which the maximum occurs in the CH_3O signal.

The reaction mechanism and the rate constants employed in the simulation of the experimental CH_3O temporal profiles are given in Table 1. With the exception of k_{3b}, all the rate constants were fixed during the simulation process. The diffusional loss rate for the CH_3 radical is taken to be equal to that of CH_3O radical, with a value of $k_{diff} = 50$ s^{-1} determined in our laboratory.[6] The rate constant of the disproportionation reaction $CH_3O + NO_2$, i.e., k_{4a}, was fixed to the value extracted at T = 298 K from the expression obtained by McCaulley et al.:[13]

$$k_{4a}(T) = 1.1 \times 10^{-11} \exp((-1200 \pm 600)\ \mathrm{K}/T)\ \mathrm{cm^3\ molecule^{-1}\ s^{-1}} \quad \text{(I)}$$

As far as the association reaction rate constant, k_{4b}, is concerned, the value fixed at room temperature corresponds to that obtained in our recent work on the $CH_3O + NO_2$ reaction: $k_{4b} = (1.41 \pm 0.05) \times 10^{-11}$ cm^3 molecule^{-1} s^{-1}.[6] The rate constant for CH_3O formation in the $CH_3 + NO_2$ reaction (k_{3a}) was fixed to the value determined by Yamada et al.[14] The rate constant for the $CH_3 + NO_2$ recombination reaction (k_{3b}) was then varied to obtain the best fit of the simulated CH_3O concentration profiles to the experimental data. This technique allows a more accurate determination of the rate constant k_{3b} than does the simultaneous variation of k_{3b} and k_{4b}. The average rate constants k_{3b} extracted from the numerical analysis of the curves at T = 298 K and at different total pressures ($p_T = 20-311$ Torr) are listed in Table 2. The uncertainties quoted in these

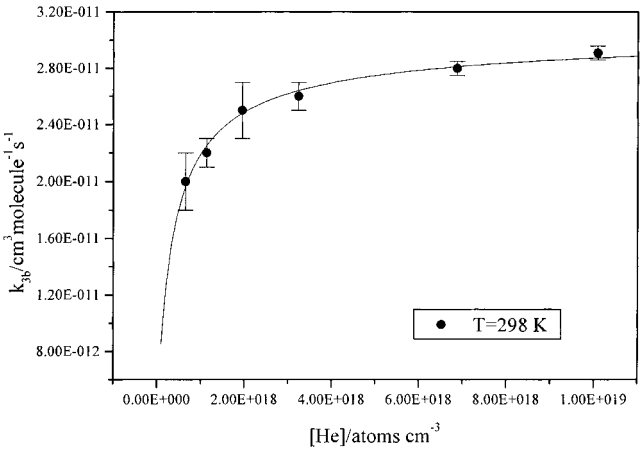

Figure 2. Falloff curve for the rate constant of the $CH_3 + NO_2 + He$ recombination reaction at room temperature and $p_T = 20-311$ Torr.

TABLE 2: Summary of the Absolute Rate Constants of the $CH_3 + NO_2 + He$ Reaction Obtained in the Fitting of the Experimental CH_3O Temporal Profiles at T = 298 K and Different Total Pressures

p_T (Torr)	[He] (10^{18} atoms cm^{-3})	$k_{3b} \pm 2\sigma$ (10^{-11} cm^3 molecule^{-1} s^{-1})
20	0.65	(2.00 ± 0.20)
35	1.13	(2.20 ± 0.10)
60	1.94	(2.50 ± 0.20)
100	3.24	(2.60 ± 0.10)
212	6.87	(2.80 ± 0.05)
311	10.08	(2.91 ± 0.05)

values are twice the standard deviation ($\pm 2\sigma$). These rate constants for the $CH_3 + NO_2$ recombination reaction were fitted to a conventional Troe expression:[15]

$$k_{3b}(\mathrm{He}) = \frac{k_{3b}^0[\mathrm{He}]}{1 + (k_{3b}^0[\mathrm{He}]/k_{3b}^\infty)} F_C^{\{1+(N^{-1}(\log(k_{3b}^0[\mathrm{He}]/k_{3b}^\infty)))^2\}^{-1}} \quad \text{(II)}$$

$$N = 0.75 - 1.27 \log F_C \quad \text{(III)}$$

where F_C is the broadening factor and k_{3b}^0 and k_{3b}^∞ are the low- and high-pressure limiting rate constants, respectively, at a given temperature. The value of F_C is fixed at 0.6, as recommended by the JPL for atmospheric reactions.[16] The falloff curve generated in the nonlinear least-squares fitting to eq II of rate constants k_{3b} obtained in this work is presented in Figure 2. The values of k_{3b}^0 and k_{3b}^∞ extracted from this analysis are

$$k_{3b}^0(T = 298\ \mathrm{K}) = (3.73 \pm 0.72) \times 10^{-28}\ \mathrm{cm^6\ molecule^{-2}\ s^{-1}}$$

$$k_{3b}^\infty(T = 298\ \mathrm{K}) = (3.26 \pm 0.40) \times 10^{-11}\ \mathrm{cm^3\ molecule^{-1}\ s^{-1}}$$

where the error limits include $\pm 2\sigma$ and estimated systematic errors in the determination of concentrations.

The numerically simulated CH_3O concentration profiles were fitted with FACSIMILE to the time-dependent LIF(CH_3O) signals obtained under the same conditions. This process allows a relationship to be established between LIF intensity and $[CH_3O]$, and this can be used in the study of the $CH_3 + O_3$ reaction (see Section 3.3).

3.2. Kinetic Study of the $CH_3O + O_3$ Reaction. Photolysis of CH_3ONO at λ = 193 nm was used as a source of CH_3O in

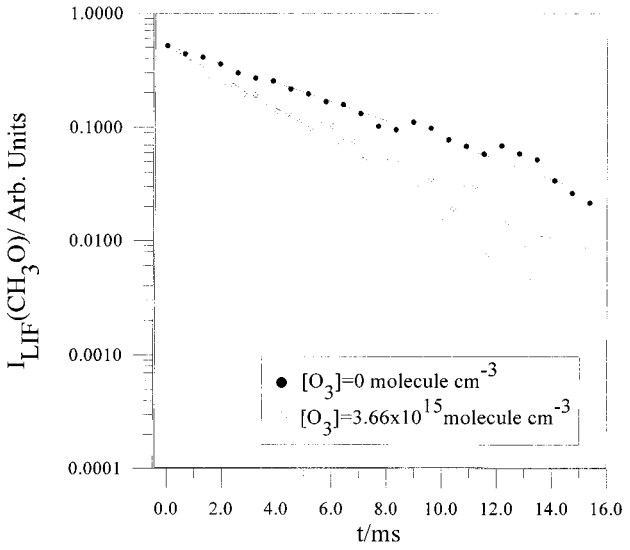

Figure 3. Semilogarithmic plots of CH_3O LIF signal obtained in the photolysis of $[CH_3ONO] = 2.1 \times 10^{14}$ molecule cm^{-3} at $\lambda = 193$ nm in the absence (○) and in the presence of $[O_3] = 3.66 \times 10^{15}$ molecule cm^{-3} (●).

order to study the kinetics of this radical both in the absence and in the presence of different ozone concentrations at 100 Torr of pressure. The CH_3O LIF temporal profiles recorded are monoexponential in all cases, as can be seen in the example ofthe semilogarithmic plots presented in Figure 3. The pseudo-first-order rate coefficients, k', obtained from the analysis of these temporal profiles are 191 and 315 s^{-1} in the absence and presence of O_3, respectively.

In the absence of reactant, a set of experiments was carried out using different precursor concentrations. In these experiments, the kinetics of CH_3O is mainly determined by diffusion (reaction 9) and reaction with its photochemical precursor, CH_3ONO:

$$CH_3O + CH_3ONO \xrightarrow{k_{10}} \text{products} \qquad (10)$$

A pseudo-first-order plot for reaction 10 is shown in Figure 4a. The slope of this linear representation gives rise to the following:

$$k_{10}(T = 298\ \text{K}) = (4.45 \pm 0.90) \times 10^{-13}\ \text{cm}^3\ \text{molecule}^{-1}\ \text{s}^{-1}$$

Similar experiments were carried out under pseudo-first-order conditions in the presence of different O_3 concentrations. Figure 4b shows an example of the linear pseudo-first-order plots obtained. The rate coefficient determined from the slope of this plot for $CH_3O + O_3$ reaction was $k_2(T = 298\ \text{K}) = (3.25 \pm 0.64) \times 10^{-14}$ cm^3 $molecule^{-1}$ s^{-1}. The mean value obtained for this reaction is

$$k_2(T = 298\ \text{K}) = (2.53 \pm 0.75) \times 10^{-14}\ \text{cm}^3\ \text{molecule}^{-1}\ \text{s}^{-1}$$

The mean value of k_2 obtained in the $CH_3ONO/O_3/He$ system was then used in the chemical model described in the next section. This model was used to determine the rate constant of CH_3O formation in reaction 1a for the $CH_3Br/O_3/He$ system.

3.3. Kinetics of the $CH_3 + O_3$ Reaction: CH_3O Yield. The rate of CH_3O formation in reaction 1a was studied under pseudo-first-order conditions with respect to the initial concentration

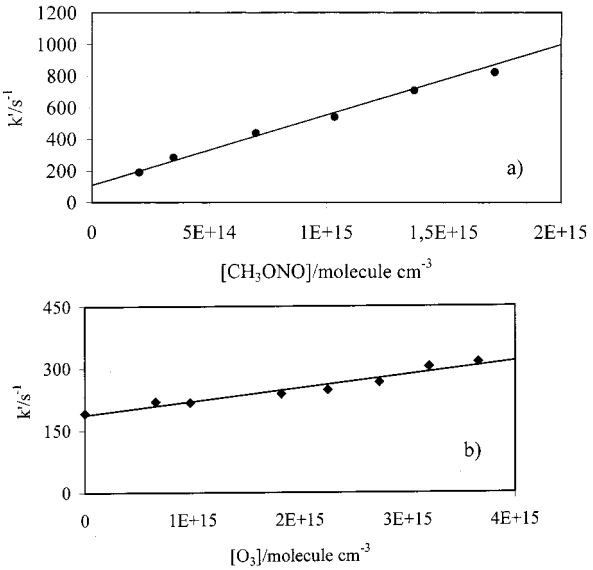

Figure 4. Pseudo-first-order plots obtained at $p_T = 100$ Torr and room temperature (a) in the absence of ozone and (b) in the presence of different $[O_3]$ using a CH_3ONO concentration of 2.1×10^{14} molecule cm^{-3}.

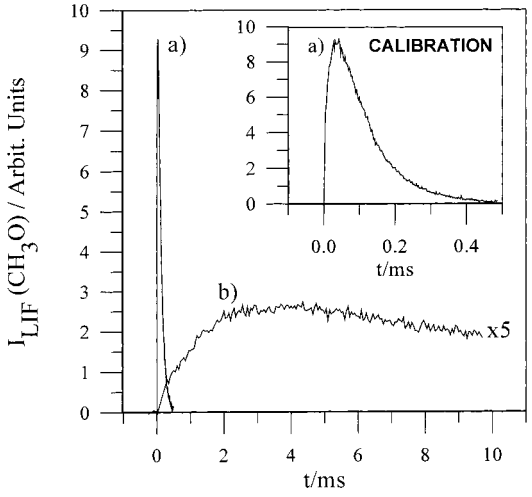

Figure 5. Comparison between time-dependent CH_3O profiles in (a) $CH_3Br(\lambda = 193\ \text{nm})/NO_2/He$ calibration system, where $[NO_2] = 3.6 \times 10^{14}$ molecule cm^{-3} and (b) $CH_3Br(\lambda = 193\ \text{nm})/O_3/He$ system, where $[O_3] = 3.1 \times 10^{14}$ molecule cm^{-3}. Experimental conditions: $[CH_3Br] = 1.92 \times 10^{14}$ molecule cm^{-3} and $[CH_3]_0 = 1.03 \times 10^{12}$ radical cm^{-3}. The inset corresponds to the $[CH_3O]$ profile presented in part a rescaled in 500 μs time.

of the CH_3 radical at room temperature and at a total pressure of 100 Torr. The difference in CH_3O concentrations formed in the calibration reaction ($CH_3 + NO_2$) and in the $CH_3 + O_3$ reaction is clearly demonstrated in Figure 5. In both cases, the same photochemical precursor (CH_3Br) was used and the same concentrations of CH_3 radical and reactant were employed. It can be seen, however, that the CH_3O signal observed for reaction 3a is about 20 times greater than that for reaction 1a. Thus, in Figure 5, the CH_3O fluorescence signal obtained in the reaction of CH_3 radicals with O_3 is multiplied by a factor of 5 in order that a better comparison can be made.

Numerical simulation of CH_3O concentration profiles was performed using the FACSIMILE computer program. This study involved different kinetic mechanisms in order to analyze the influence of different reactions on the values of k_1 and k_{1a} derived from the fitting of the calculated profiles to the LIF CH_3O signal.

TABLE 3: Reaction Scheme Used in the Analysis of the CH_3O Temporal Profiles Obtained at $T = 298$ K and 100 Torr in $CH_3Br(\lambda = 193$ nm)/O_3/He System

second-order reactions	k (298 k) (cm^{-3} $molecule^{-1}$ s^{-1})	reference
basic mechanism		
$CH_3 + O_3 \rightarrow CH_3O + O_2$	k_{1a} = variable	this work
$CH_3 + O_3 \rightarrow$ products	$k_1 = 2.2 \times 10^{-12}$	this work
$CH_3O + O_3 \rightarrow$ products	$k_2 = 2.53 \times 10^{-14}$	this work
$CH_3 + CH_3 \rightarrow C_2H_6$	$k_{11} = 8.0 \times 10^{-11}$	17
$CH_3O + Br \rightarrow$ products	$k_{12} = 7 \times 10^{-11}$	18
$CH_3 \rightarrow$ diffusion	$k_{diff} = 50^a$	this work
$CH_3O \rightarrow$ diffusion	$k_{diff} = 50^a$	6
Additional O Atom Reactions Included in the Extended Mechanism		
$O(^3P) + CH_3O \rightarrow$ products	2.5×10^{-11}	30
$O(^3P) + CH_3 \rightarrow CH_3O$	2.6×10^{-14}	31
$O(^3P) + CH_3 \rightarrow CH_2O + H$	$k_{16} = 1.1 \times 10^{-10}$	32
$O(^1D) + CH_3Br \rightarrow BrO + CH_3$	$k_{13} = 7.78 \times 10^{-11}$	19, 20
$O(^1D) + CH_3Br \rightarrow O(^3P) + CH_3Br$	1.5×10^{-11}	19
$O(^1D) + O_3 \rightarrow 2O_2$	1.2×10^{-10}	21
$O(^1D) + O_3 \rightarrow 2O + O_2$	1.2×10^{-10}	21
Other Additional Reactions		
$Br + O_3 \rightarrow BrO + O_2$	1.1×10^{-12}	16
$BrO + CH_3O \rightarrow$ products	3.8×10^{-11}	18
$CH_3O + CH_3 \rightarrow$ products	2.63×10^{-11}	33

[a] First-order rate coefficients, in inverse seconds.

The most important reactions are included in the *basic mechanism* (see Table 3). This chemical model consists of reactions 1a, 1, and 2, together with CH_3 recombination, reaction of CH_3O with Br atoms, and diffusion of CH_3 and CH_3O out of the detection zone. For k_2, the value determined above in Section 3.2 of this work was used, whereas for the methyl radical recombination reaction,

$$CH_3 + CH_3 \xrightarrow{k_{11}} C_2H_6 \qquad (11)$$

the value obtained by De Avillez et al.[17] was used, because in most cases $[CH_3]_0$ was greater than 1×10^{12} radical cm^{-3}. However, the recombination reaction of CH_3O radicals was not included in this model, because the concentrations generated were low ($[CH_3O]_{max} \leq 5 \times 10^{11}$ radical cm^{-3}) and were therefore influential to only a small extent. For the reaction

$$CH_3O + Br \xrightarrow{k_{12}} \text{products} \qquad (12)$$

the rate coefficient determined by Aranda et al. was assumed.[18]

Although the excimer laser photolysis wavelength selected was 193 nm rather than 248 nm, to minimize O_3 dissociation, the reactions of oxygen atoms generated in the photolysis ($O(^3P)$ and $O(^1D)$) are considered in the *extended mechanism* presented in Table 3. As the experiments were performed in He, where the quenching of $O(^1D)$ produced in the photolysis of ozone is slow, an additional source of CH_3 could arise from the rapid reaction of CH_3Br with $O(^1D)$,[19]

$$CH_3Br + O(^1D) \xrightarrow{k_{13}} \text{products} \qquad (13)$$

where CH_3 is formed with a yield of 0.44 ± 0.05.[20] This reaction was also considered in the extended mechanism together with the reaction of $O(^1D)$ with O_3[21] and the quenching of excited O in the presence of CH_3Br.[19]

Additional secondary chemistry included in the extended mechanism (see Table 3) was the reactions of CH_3O with CH_3 and BrO,[18] as well as the reaction of Br with O_3.[16] Other bromine and crossed radical reactions considered showed a negligible influence on the determination of k_1 and k_{1a}.

The possible effect of the reaction of CH_3 with O_2,

$$CH_3 + O_2 + M \xrightarrow{k_{14}} CH_3O_2 + M \qquad (14)$$

on the determination of k_1 and k_{1a} was negligible at the O_2 concentrations present in our system, with the only oxygen arising from the presence of O_2 in the aged O_3 mixtures (see Experimental Section).

Initially, reaction 1 was considered to proceed only through reaction 1a to form CH_3O. In this case, varying the branching ratio, k_{1a}/k_1, would only affect the calculated absolute concentration of CH_3O but not the shape of the CH_3O profile from which the total rate coefficient k_1 was determined upon optimizing only this parameter in the simulation process.

The rate coefficients k_1 obtained with the extended mechanism differ by less than 5% from those obtained using the *basic mechanism* and both provide a good description of the experimental profiles. The mean value of k_1 obtained from the analysis of the experimental data is

$$k_1(T = 298 \text{ K}) = (2.2 \pm 0.3) \times 10^{-12} \text{ cm}^3 \text{ molecule}^{-1} \text{ s}^{-1}$$

The rate coefficients k_1 and k_2 determined in this work were included in the kinetic mechanisms considered. From this approach, we derived k_{1a} and the CH_3O yield by comparing the time dependencies of the CH_3O concentration profiles obtained by photolysis of CH_3Br/NO_2 and CH_3Br/O_3 under the same experimental conditions (concentration, pressure, temperature, flow conditions, and laser fluence). The relationship between I_{LIF} and $[CH_3O]$ obtained in the kinetic study of the $CH_3 + NO_2$ reaction (Section 3.1) was used to calibrate the CH_3O LIF signal registered in the study of the $CH_3 + O_3$ reaction. In this calibration, the CH_3O LIF signal was transformed into CH_3O concentrations at different times, and the data were input into the FACSIMILE program in order to analyze the concentration−time profiles obtained. This analysis was performed using the kinetic mechanisms presented in Table 3 and by varying only the parameter k_{1a}. This numerical analysis allows the influence of several reactions to be determined in the CH_3O yield obtained in the $CH_3 + O_3$ reaction.

An example of these temporal profiles (dots) and the corresponding best fit using the extended mechanism (line) is shown in Figure 6. In this case, the value of k_{1a} extracted from the analysis is $(9.91 \pm 0.10) \times 10^{-14}$ cm^3 $molecule^{-1}$ s^{-1}. If only the basic mechanism is considered, the best fit of the experimental data gives $k_{1a} = (9.47 \pm 0.12) \times 10^{-14}$ cm^3 $molecule^{-1}$ s^{-1}, where the quoted $\pm 2\sigma$ errors reflect only the precision of the fit.

In all cases, the fitting of the calculated profiles to the experimental data is reasonably good and is slightly better with the extended mechanism. The difference in the derived value of k_{1a} is less than 5% and is smaller than the estimated uncertainty associated with systematic errors in the determination of concentrations. Taking into account all the results and the estimated experimental errors, the average value derived for the rate constant of reaction 1a is

$$k_{1a} = (9.68 \pm 1.10) \times 10^{-14} \text{ cm}^3 \text{ molecule}^{-1} \text{ s}^{-1}$$

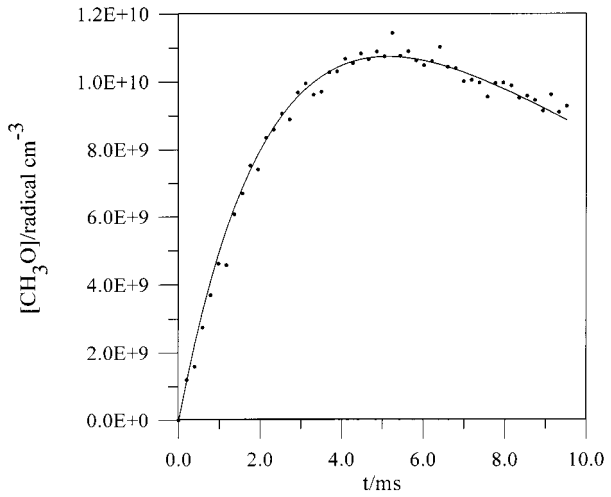

Figure 6. Numerical analysis of the CH_3O concentration profiles recorded in the reaction of $[CH_3]_0 = 7.8 \times 10^{11}$ radical cm^{-3} with ozone ($[O_3] = 1.1 \times 10^{14}$ molecule cm^{-3}) at $T = 298$ K. Several kinetic mechanisms are used in order to find the best fit of the curve (see text).

According to these results, the yield of the CH_3O formation channel in the reaction of CH_3 with O_3, $\phi_{CH_3O} = k_{1a}/k_1$, is

$$\phi_{CH_3O} = (0.044 \pm 0.013)$$

Thus, reaction 1a accounts for about 4.4% of the global CH_3 loss by reaction with O_3.

The influence of the different LIF quenching rates by O_3 and NO_2 was not determined precisely. Nevertheless, considering that both species are angular triatomic molecules of similar size and structure, and taking into account the recent study by Kukui et al.[22] in which a maximum correction of about 10% was determined for the different rates of CH_3O fluorescence quenching by CH_3I and DMDS, we estimate that in the present study the correction should be smaller and is included in the uncertainty ranges given for ϕ_{CH_3O}.

On the other hand, the estimated influence on the determination of the CH_3O yield of a 10% uncertainty in the initial $[CH_3]$ value is less than 8%, and the effect of the rate constants uncertainties used for reactions 1−4 is smaller than 3%.

4. Discussion

4.1. Kinetics of the $CH_3 + NO_2$ Reaction: CH_3O Calibration. The product of the recombination reaction 3b could be either CH_3ONO or CH_3NO_2. Yamada et al. did not observe CH_3NO_2 in the reaction $CH_3 + NO_2$.[14] This fact is in sensible agreement with the small CH_3NO_2 yield (0.04−0.07) obtained by McCaulley et al. at low pressures (0.5−1 Torr).[23] Combining the rate constant determined by Yamada et al.[14] for the bimolecular process (reaction 3a) with their data for the CH_3NO_2 yields, McCaulley et al.[23] estimated the low-pressure limiting rate constant k_{3b}^0 given in Table 4. It can be seen from the data in this table that the value of k_{3b° obtained in this work is

$$k_{3b}^0(T = 298\ \text{K}) = (3.73 \pm 0.72) \times 10^{-28}\ \text{cm}^6\ \text{molecule}^{-2}\ \text{s}^{-1}$$

which is in fair agreement with that obtained by McCaulley et al.[23] as well as in other investigations.[22,24,25] On the other hand, the value obtained in this work for k_{3b}^∞

$$k_{3b}^\infty(T = 298\ \text{K}) = (3.26 \pm 0.40) \times 10^{-11}\ \text{cm}^3\ \text{molecule}^{-1}\ \text{s}^{-1}$$

is in good agreement, within the uncertainty ranges given, with those determined by Glänzer and Troe[24] using a shock-tube system at high temperatures in Ar ($T = 1100-1400$ K) and with recent LP/LIF studies performed at room temperature in He[22] and as a function of temperature in Ar.[25] To compare the rate constants obtained in Ar with those obtained in He, the data in Ar have been assigned an equivalent pressure of He to reflect the relative third-body efficiencies of these bath gases ($\beta_C(\text{He}) = 0.07$ and $\beta_C(\text{Ar}) = 0.12$).[26]

TABLE 4: Comparison of the Low- and High-Pressure Limiting Rate Constant, k_{3b}^0 and k_{3b}^∞ for the $CH_3 + NO_2 +$ He Association Reaction at Room Temperature

carrier gas	$(k_{3b}^0 \pm 2\sigma) \times 10^{28}$ (cm^6 $molecule^{-2}$ s^{-1})	$(k_{3b}^\infty \pm 2\sigma) \times 10^{11}$ (cm^3 $molecule^{-2}$ s^{-1})	reference
He	(2.73 ± 0.72)	(3.26 ± 0.40)	this work[a]
	(2.17 ± 1.20)	(3.45 ± 0.50)	this work[b]
	(4.2 ± 0.5)	(2.0 ± 1.0)	22
	(0.6 ± 0.2)		23
Ar	9.89	3.43	24
	(3.2 ± 1.3)	(4.3 ± 0.4)	25

[a] $p_T = 20-311$ Torr. [b] $p_T = 12-612$ Torr (Composite Dataset).

The strong pressure dependence of k_{3b} observed in this work was not evident in the kinetic study of reaction 3 made by Biggs et al. in a discharge-flow system.[27] These authors found k_3 to be independent of pressure between 1 and 7 Torr, with a rate constant of $(2.3 \pm 0.3) \times 10^{-11}$ cm^3 $molecule^{-1}$ s^{-1}. This may reflect the fact that the measurements were not carried out over a extended pressure range, and that the effect at low pressures is partially disguised by the presence of the fast, pressure independent bimolecular reaction 3a.

If all data sets, which cover a pressure range of 12−612 Torr, are included in the fitting procedure, using Troe formalism, the low- and high-pressure limiting rate constants obtained are

$$k_{3b}^0(T = 298\ \text{K}) = (2.17 \pm 1.20) \times 10^{-28}\ \text{cm}^6\ \text{molecule}^{-2}\ \text{s}^{-1}$$

$$k_{3b}^\infty(T = 298\ \text{K}) = (3.45 \pm 0.50) \times 10^{-11}\ \text{cm}^3\ \text{molecule}^{-1}\ \text{s}^{-1}$$

The agreement of these results, within the error limits, with the values of k_{3b}^0 and k_{3b}^∞ extracted from the analysis of the rate constants listed in Table 2 denotes that both limiting rate constants are determined reasonably well using our data between 20 and 311 Torr. Error limits include $\pm 2\sigma$ and estimated systematic errors in the determination of concentrations. Nevertheless, the fit to the composite dataset must give more reliable values, especially for the low-pressure limit.

4.2. Kinetic Study of the $CH_3O + O_3$ Reaction. The only previous study of reaction 10 reported in the literature was performed in Ar at total pressures between 100 and 342 Torr using a shock wave system.[28] The CH_3O generated by thermal decomposition of CH_3ONO was monitored by chemiluminescence. The authors reported a value of $k_{10} = 4.15 \times 10^{-12}$ cm^3 $molecule^{-1}$ s^{-1} independent of temperature in the range 700−900 K. The value determined in this study is consistent with a weak temperature dependence of k_{10}.

On the other hand, as far as we know, the only previous value of k_2 reported in the literature is an upper limit, indirectly determined by Simonaitis and Heicklen.[3] A value of $k_2 < 2 \times 10^{-15}$ cm^3 molecule^{-1} s^{-1} was estimated at room temperature using the $O_3(\lambda = 253.7\ nm)/CH_4/O_2$ chemical system. This value is 10 times lower that the value directly determined for the first time in the present study.

4.3. Kinetic Study of the $CH_3 + O_3$ Reaction: CH_3O Yield. As stated in Results, the influence of the secondary chemistry, which was not included in the basic mechanism, for the determination of k_1 and k_{1a} from the kinetic data of CH_3O radicals was small (less than 5%) at the concentrations present in our system. Although a CH_3O yield was not determined in Cronkhite and Wine's work[20] on the reaction of $CH_3Br + O(^1D)$, we considered the possibility of direct CH_3O formation in this reaction. However, such as mechanism is not consistent with the experimental CH_3O temporal profiles observed.

As mentioned in the Introduction, the kinetics of the $CH_3 + O_3$ reaction have been the subject of three previous studies.[1-3] Simonaitis and Heicklen[3] estimated the ratio of rate constants for reactions 1 and 14, obtaining values of $k_1/k_{14} = 1.17$ at -52 °C and 2.17 at 25 °C. Considering $k_{14} = 4.3 \times 10^{-13}$ cm^3 molecule^{-1} s^{-1} at the high-pressure limit and assuming that this value is independent of temperature, they obtained the Arrhenius expression

$$k_1(T) = 5.4 \times 10^{-12} \exp(-530/T)\ \text{cm}^3\ \text{molecule}^{-1}\ \text{s}^{-1} \qquad \text{(IV)}$$

yielding $k_1(T = 298\ \text{K}) = 9.1 \times 10^{-13}$ cm^3 molecule^{-1} s^{-1}, more than two times slower than the room-temperature value determined in this work ($k_1 = (2.2 \pm 0.3) \times 10^{-12}$ cm^3 molecule^{-1} s^{-1}). Information regarding the products was not given in that previous study, but Simonaitis and Heicklen[3] proposed that vibrationally excited CH_3O formation in reaction 1a was the major channel (if not the exclusive channel) by which the $CH_3 + O_3$ reaction proceeds. The basis of this proposal was that the large preexponential factor obtained in the Arrhenius expression favors a linear transition state yielding CH_3O and O_2.

Thermodynamically, the possibility exists that reaction 1 proceeds through different channels:

$$CH_3 + O_3 \xrightarrow{k_{1a}} CH_3O + O_2 \quad \Delta H = -280\ \text{kJ mol}^{-1} \qquad \text{(1a)}$$

$$CH_3 + O_3 \xrightarrow{k_{1b}} CH_2O + HO_2 \quad \Delta H = -374\ \text{kJ mol}^{-1} \qquad \text{(1b)}$$

$$CH_3 + O_3 \xrightarrow{k_{1c}} HCOOH + OH \quad \Delta H = -621\ \text{kJ mol}^{-1} \qquad \text{(1c)}$$

Other reaction pathways are

$$CH_3 + O_3 \xrightarrow{k_{1d}} CH_2O_2 + OH \qquad \text{(1d)}$$

$$CH_3 + O_3 + He \xrightarrow{k_{1e}} CH_3O_3 + He \qquad \text{(1e)}$$

In the study of Washida et al.[1], methyl radicals were generated in the reaction of oxygen atoms with ethylene in a flow system

$$O + C_2H_4 \rightarrow CH_3 + CHO \qquad (15)$$

and the absolute rate constant for reaction 1 is obtained as a result of the competition among O, O_2, and O_3 for CH_3. Observing the effect of added O_3 on the steady-state concentration of CH_3, they determined the ratio $k_1/k_{16} = 5.1 \times 10^{-3}$, where k_{16} refers to the reaction:

$$CH_3 + O \xrightarrow{k_{16}} CH_2O + H \qquad (16)$$

Using a value of 1.38×10^{-10} cm^3 molecule^{-1} s^{-1} for k_{16}, they calculated $k_1 = (7.0 \pm 2.7) \times 10^{-13}$ cm^3 molecule^{-1} s^{-1} and found this to be independent of total pressure ($p_T = 2-6$ Torr). This value is in fair agreement with that obtained by Simonaitis and Heicklen[3] but is approximately three times slower than the value determined in this work. This pressure independence shows that the addition reaction channel (1e), if indeed it occurs, must be in the high-pressure limit under our experimental conditions ($p_T = 100$ Torr). Washida et al.[1] did not detect formic acid, HCOOH, by mass spectrometry, although the ionization potential of this compound is smaller (11.05 eV) than that of the ionization source employed (11.83 and 11.62 eV). However, a large signal at $m/z = 30$ due to formaldehyde, CH_2O, was observed but cannot be assigned exclusively to reaction channel 1b because the presence of CH_2O could be due to the contribution of other reactions such as

$$CH_3O_2 + O \rightarrow CH_2O + HO_2 \qquad (17)$$

$$CH_3O + O \rightarrow CH_2O + OH \qquad (18)$$

$$CH_3O + O_2 \rightarrow CH_2O + HO_2 \qquad (19)$$

On the other hand, Ogryzlo et al.[2] determined the rate constant k_1 at 2 Torr as a function of temperature ($T = 243-384$ K) by monitoring CH_3 decay using photoionization mass spectrometry detection coupled to a flash photolysis system. The corrected rate constants for the pressure drop between the reaction cell and the capacitance manometer gave the following Arrhenius expression[29]

$$k_1(T) = (5.1 \pm 1.6) \times 10^{-12} \exp((-210 \pm 84)/T)\ \text{cm}^3\ \text{molecule}^{-1}\ \text{s}^{-1} \qquad \text{(V)}$$

yielding a value of $k_1 = 2.5 \times 10^{-12}$ cm^3 molecule^{-1} s^{-1} at room temperature. This value is in good agreement with that determined in this work. Information concerning the products of reaction 1 was not obtained in that kinetic study, and a signal was not observed at $m/z = 31$, corresponding to CH_3O radical, although the authors were not sure that this radical would be photoionized by the 123.6 nm radiation used.

The LIF detection of CH_3O radicals in this reaction, reported for the first time in this work, reveals that reaction channel 1a occurs only to a small extent.

5. Conclusions and Atmospheric Implications

In this paper, we present the first determination of the CH_3O yield in the reaction of CH_3 with O_3 at room temperature and 100 Torr of total pressure. The low branching ratio observed in this study, $\phi_{CH_3O} \cong 0.044$, can be explained by the formation of highly vibrationally excited CH_3O and the subsequent prompt dissociation to produce formaldehyde, CH_2O, and H atoms

$$CH_3O^{\#} \rightarrow CH_2O + H \qquad (20)$$

but also by the direct formation of $CH_2O + HO_2$ in reaction channel 1b.

We also report the first direct measurement of the rate constant for the reaction $CH_3O + O_3$ at room temperature and

100 Torr. The value obtained using the system $CH_3ONO(\lambda = 193$ nm)/O_3/He is $k_2(T = 298\ K) = (2.53 \pm 0.75) \times 10^{-14}$ cm^3 molecule^{-1} s^{-1}.

In polluted environments, the estimated tropospheric lifetime for the CH_3 radical in the presence of O_3 (150 ppbv) and NO_2 (30 ppbv) is less than 1 s. This value is estimated, taking into account the global rate constant for the $CH_3 + O_3$ reaction obtained in this work ($k_1 = 2.2 \times 10^{-11}$ cm^3 molecule^{-1} s^{-1}) and the rate constant of the reaction $CH_3 + NO_2 +$ He at atmospheric pressure using the values of k_{3b}^0 and k_{3b}^∞ extracted in this work ($k_{3b} = 5.7 \times 10^{-11}$ cm^3 molecule^{-1} s^{-1}). In the natural atmosphere, the reaction of the CH_3 radical with O_3 (30 ppbv) dominates over the reaction with NO_2 (1 ppbv). However, due to the great abundance of O_2 (5×10^{18} molecule cm^{-3}), the major CH_3 removal process in the atmosphere is reaction 14.

Acknowledgment. The authors gratefully thank the European Commission (EL CID Project Number EVK2-CT-1999-00033) and the D. G. E. S (Project P97-0432) for supporting this work.

References and Notes

(1) Washida, N.; Akimoto, H.; Okuda, M. *J. Chem. Phys.* **1980**, *73*, 1673.

(2) Ogryzlo, E. A.; Paltenghi, R.; Bayes, K. D. *Int. J. Chem. Kinet*. **1981**, *13*, 667.

(3) Simonaitis, R.; Heicklen, J. *J. Chem. Phys.* **1975**, *79*, 298.

(4) Martínez, E.; Albaladejo, J.; Jiménez, E.; Notario, A.; Aranda, A. *Chem. Phys. Lett*. **1999**, *308*, 37.

(5) Martínez, E.; Albaladejo, J.; Jiménez, E.; Notario, A. *Atmos. Environ.* **2000**, *34*, 5295.

(6) Martínez, E.; Albaladejo, J.; Jiménez, E.; Notario, A.; Díaz de Mera, Y. *Chem. Phys. Lett*. **2000**, *329*, 191.

(7) Ionue, G.; Akimoto, H.; Okuda, M. *J. Chem. Phys*. **1980**, *72*, 1769.

(8) Gillotay, D.; Simon, P. C. *Ann. Geophys.*. **1988**, *6*, 211.

(9) Talukdar, R. K.; Vaghjiani, G. L.; Ravishankara, A. R. *J. Chem. Phys*. **1992**, *96*, 8194.

(10) Maricq, M. M.; Wallington, T. J.; *J. Phys. Chem*. **1992**, *96*, 986.

(11) WMO, *Atmospheric Ozone: 1985 World Meterological Organization Global Ozone Research and Monitoring Project*, Report N*o*. 16, 1986; Geneva, National Aeronautics and Space Administration.

(12) Turnipseed, A. A.; Vaghjiani, G. L.; Gierczak, T.; Thompson, J. E.; Ravishankara, A. R. *J. Chem. Phys*. **1991**, *98*, 3244.

(13) McCaulley, J. A.; Anderson, S. M.; Jeffries, J. B.; Kaufman, F. *Chem. Phys. Lett*. **1985**, *115*, 180.

(14) Yamada, F.; Slagle, I. R.; Gutman, D. *Chem. Phys. Lett*. **1981**, *83*, 409.

(15) Troe, J. *J. Chem. Phys*. **1977**, *66*, 4758.

(16) DeMore, W. B.; Sanders, S. P.; Golden, D. M.; Hampson, R. F.; Kurylo, M. J.; Howard, C. J.; Ravishankara, A. R.; Kolb, C. E.; Molina, M. J. *Chemical Kinetics and Photochemical Data for Use in Stratospheric Modeling*. Evaluation N*o*. 12, 1997; Jet Propulsion Laboratory, Pasadena, California.

(17) De Avillez, R.; Baulch, D. L.; Pilling, M. J.; Robertson, S. H.; Zeng, G. *J. Phys. Chem. A.* **1997**, *101*, 9681.

(18) Aranda, A.; Daele, V.; Le Bras, G.; Poulet, G. *Int. J. Chem. Kinet*. **1998**, *30*, 249.

(19) Thompson, J. E.; Ravishankara, A. R. *Int. J. Chem. Kinet*. **1993**, *25*, 479.

(20) Cronkhite, J. M.; Wine, P. H. *Int. J. Chem. Kinet*. **1998**, *30*, 555.

(21) Davenport, J. E.; Ridley, B.; Schiff, H. I., Welge, K. H. *J. Chem. Soc., Faraday Discuss.* **1972**, *53*, 230.

(22) Kukui, A.; Boustrot, V.; Laverdet, G.; Le Bras, G. *J. Phys. Chem A.* **2000**, *104*, 935.

(23) McCaulley, J. A.; Moyle, A. M.; Golde, M. F.; Anderson, S. M.; Jeffries, J. B.; Kaufman, F. *J. Chem. Soc. Faraday Trans*. **1990**, *86*, 4001.

(24) Glänzer, K.; Troe, J. *Ber. Bunsen-Ges. Phys. Chem*. **1974**, *78*, 182.

(25) Wollenhaupt, M.; Crowley, J. N. *J. Phys. Chem. A.* **2000**, *104*, 6429.

(26) Frost, M. J.; Smith, I. W. M. *J. Chem. Soc., Faraday Trans*. **1990**, *86*, 1751.

(27) Biggs, P.; Canosa-Mas, C. E.; Fracheboud, J. M.; Parr, A. D.; Shallcross, D. E.; Wayne, R. P.; Caralp, F. *J. Chem. Soc., Faraday Trans*. **1993**, *89*, 4163.

(28) Zaslonko, I. S.; Mukoseev, Y. K.; Tyurin, A. N. *Kinet. Catal*. **1988**, *29*, 244.

(29) Paltenghi, R.; Ogryzlo, E. A.; Bayes, K. D. *J. Phys. Chem*. **1984**, *88*, 2595.

(30) Baulch, D. L.; Cobos, C. J.; Cox, R. A.; Esser, C.; Frank, P.; Just, T.; Kerr, J. A.; Pilling, M. J.; Troe, J.; Walker, R. W.; Warnatz, J. *J. Phys. Chem. Ref. Data.* **1992**, *21*, 411.

(31) Dean, A. M.; Westmoreland, P. R. *Int. J. Chem. Kinet*. **1987**, *19*, 207.

(32) Zellner, R.; Hartman, D.; Karthauser, J.; Rhasa, D.; Weibring, G. *J. Chem. Soc., Faraday Trans.* 2 **1988**, *84*, 549.

(33) Heicklen, J. *Adv. Photochem*. **1988**, *14*, 177.